Available online at www.sciencedirect.com
ScienceDirect
Journal of Nuclear Materials 374 (2008) 158–167
journal of nuclear materials
www.elsevier.com/locate/jnucmat

Thermal decomposition and kinetic analysis of sodium propoxides

K. Chandran [a], M. Kamruddin [b], P.K. Ajikumar [b], A. Gopalan [c], V. Ganesan [a,*]

[a] *Materials Chemistry Division, Indira Gandhi Centre for Atomic Research, Kalpakkam 603 102, India*
[b] *Materials Science Division, Indira Gandhi Centre for Atomic Research, Kalpakkam 603 102, India*
[c] *Department of Industrial Chemistry, Alagappa University, Karaikudi 630 003, India*

Received 24 April 2007; accepted 6 August 2007

Abstract

Sodium *n*-propoxide and sodium *iso*-propoxides were synthesized and characterized. Thermal decomposition of these compounds was studied using thermogravimetric technique (TGA) coupled with mass spectrometry (MS) under non-isothermal and isothermal conditions. Various analytical techniques namely atomic emission spectroscopy (AES), infrared spectroscopy (IR), powder X-ray diffraction (XRD), elemental and volumetric analyses were employed to characterize these compounds and their decomposition residues. Kinetic parameters, namely, the activation energy and pre-exponential factor were deduced from the dynamic TGA and MS data. The activation energies derived from isothermal runs for the thermal decomposition of sodium *n*-propoxide and sodium *iso*-propoxide were 151.45 ± 2.16 and 128.07 ± 3.44 kJ mol^{-1}, respectively. Decomposition of sodium *n*-propoxide and sodium *iso*-propoxide results in the formation of gaseous products of saturated and unsaturated hydrocarbons leaving behind residue consisting of sodium carbonate, sodium hydroxide and free carbon.

PACS: 81.70.P; 82.30.L; 61.10; 82.80

1. Introduction

Liquid sodium is used as coolant and stainless steels as structural materials in fast reactors systems [1–3]. The physical contact between these two materials at reactor operating temperatures leads to formation of a thin adherent layer of sodium over the surface of the steel components in the coolant circuit due to wetting. Though wetting favours heat exchanging efficiency in the core and intermediate heat exchanger (IHX) regions, it adversely affects the components and maintenance personnel due to high chemical reactivity of sodium with moisture in addition to radiation dose in the case of primary components. During reactor maintenance, some of the stainless steel components are required to be taken out of the reactor for maintenance or replacement. Exposure of sodium wetted components to air could lead to fire and possible explosion as the reaction between sodium and moisture present in air is highly exothermic in nature. In addition to being a fire hazard, the reaction also adversely affects the mechanical properties of the steel components due to the formation of sodium hydroxide resulting in caustic stress corrosion. To overcome these problems, generally, water vapour nitrogen process (WVN) is followed for cleaning sodium from large components such as pumps, IHXs, sub-assemblies, etc. and alcohol process for cleaning small and delicate components like bellow sealed valves, impurity monitoring devices, sampling equipments, gripper tools, etc. [4,5]. Various alcohols namely, methanol [6], ethanol [7,8], Jaysol SS [9], propanol [10,11], butyl cellosolve (butoxy ethanol) [12,13] and ethyl carbitol (diethylene glycol mono ethyl ether or 2,2′ethoxy ethoxy ethanol) [14,15] are used as sodium cleaning agents world wide. Run-away reactions leading to accident reported in the literature when ethyl carbitol was used for sodium cleaning purpose have been postulated to be due to the thermal instability of

* Corresponding author. Tel.: +91 44 27480219; fax: +91 44 27480065.
E-mail address: ganesh@igcar.gov.in (V. Ganesan).

0022-3115/$ - see front matter © 2007 Published by Elsevier B.V.
doi:10.1016/j.jnucmat.2007.08.001

the reaction products of sodium and ethyl carbitol [14,15]. The lack of such data, in the literature, on the decomposition of sodium alkoxides, namely, sodium methoxide, sodium ethoxide, sodium *n*-propoxide and sodium *iso*-propoxide, the common reaction products encountered during the sodium cleaning operation employing the widely used ethanol and propanol solvents, enthused the authors to initiate a study on thermal decomposition and kinetic analysis of these alkoxides. The thermal stability data of these alkoxides is highly desirable to arrive at a safe temperature window for the sodium cleaning operation. The present work focuses and reports for the first time, the thermal decomposition studies of sodium *n*-propoxide and sodium *iso*-propoxide and the kinetic parameters, namely, activation energy and pre-exponential factor derived from the decomposition data.

2. Experimental

2.1. Chemicals

Nuclear grade sodium (purity 99.5%) from Alkali Metals, India, was further purified by vacuum distillation. AR grade *n*-propanol (purity >99.5%) from S.D. Fine Chemicals, India, and high pressure liquid chromatography (HPLC) grade *iso*-propanol (purity 99.7%) from Ranbaxy Laboratories, India, were further purified by distillation [16]. These chemicals were used for the preparation of sodium *n*-propoxide and sodium *iso*-propoxide.

2.2. Preparation of compound

The formation and subsequent separation of pure sodium alkoxides can be represented by the following reactions:

$$\mathrm{Na} + \mathrm{ROH}_{\mathrm{excess}} \rightarrow [\mathrm{RONa}]_{\mathrm{ROH}} + 1/2\mathrm{H}_2; \quad \text{where R} = n \text{ and } \textit{iso}\text{-propyl}, \tag{1}$$

$$[\mathrm{RONa}]_{\mathrm{ROH}} \xrightarrow{\text{Vacuum distillation}} \mathrm{RONa}. \tag{2}$$

The detailed methods of preparation and characterization of these alkoxides were reported elsewhere [17].

2.3. TGA-MS measurements

Thermogravimetric analyzer model SETSYS 16/18 of Setaram, France, was used in the present work for simultaneous TGA-MS studies. The detailed descriptions of the system and the experimental procedure are reported elsewhere [18].

2.4. Characterisation of residue

2.4.1. X-ray diffraction analysis

X-ray diffractometer of STOE, Germany, was employed to characterize these sodium alkoxides, their decomposition residues and the insoluble black particles. XRD pattern was recorded at room temperature using Cu Kα (λ:1.5406 Å) radiation. The samples were loaded in Lindemann glass capillaries and sealed with paraffin wax in argon atmosphere glove box to protect them from moisture. The XRD patterns were recorded in the angular range of 5–65° with a step size of 0.05° and scan rate of 10 s per step.

2.4.2. Infrared analysis

Fourier transform infrared spectrometer model MB100 of BOMEM, USA, was employed for recording IR spectra of these compounds, their decomposition residues and insoluble content of black particles. Sodium *n*-propoxide was mixed with spectroscopic grade KBr powder and pelletised by uniaxial pressing. The pellet was sandwiched between two ZnSe windows fitted in a leak tight sample holder to protect the sample from moisture. All these operations were carried out inside an argon atmosphere glove box. The IR spectrum of the sample thus prepared was recorded in the range of 4000–400 cm^{-1} at 4 cm^{-1} resolution. Similar procedure was followed for recording IR spectra of sodium *iso*-propoxide, decomposition residue of these compounds and the insoluble portions of decomposition residues. To compare the spectral features of the residue, IR spectrum of GR grade sodium carbonate was also recorded.

2.4.3. Estimation of sodium carbonate and sodium hydroxide

Standard lime water test was performed to confirm the presence of carbonate radical in the decomposition residue of sodium *n*-propoxide and sodium *iso*-propoxide. Sodium carbonate and sodium hydroxide contents were estimated by volumetric titration method. For this purpose, about 100 mg each of residue was dissolved in distilled water, filtered and the filtrate was titrated against the standard hydrochloric acid using methyl orange or phenolphthalein as indicator to find the total alkalinity and sodium hydroxide alkalinity, respectively. The estimated quantities of sodium carbonate and sodium hydroxide are given in Table 1. The values are the mean of six measurements and the

Table 1
Sodium content estimated from the sodium carbonate and sodium hydroxide (volumetric analysis) of the residues along with the insoluble content

Decomposition residue	Soluble content (wt%)			Insoluble content (wt%)		Sodium content (wt%)		
	Na_2CO_3	NaOH	Total	Calculated	Observed	From Na_2CO_3	From NaOH	Total
Sodium *n*-propoxide	45.45	35.42	80.87	19.13	18.84	19.72	20.37	40.09
Sodium *iso*-propoxide	43.07	32.62	75.69	24.31	19.78	18.69	18.77	37.46

errors involved in the measurements were of the order of 2–3%.

During the above experiments some insoluble black particles were noticed. To estimate the soluble and insoluble contents of these residues, about 110–150 mg of the decomposition residue of sodium *n*-propoxide and sodium *iso*-propoxide were dissolved independently in distilled water, hydrochloric acid and in ether. The insoluble black particles were observed in case of water and hydrochloric addition, which were examined by powder-XRD, IR and CHNS methods.

3. Results and discussion

Fig. 1(a) and (b) shows the IR spectrum and XRD pattern of sodium *iso*-propoxide obtained in the present study, while that of sodium *n*-propoxide are reported elsewhere [17]. Absence of spectral features around 3500 and 1600 cm^{-1} region clearly shows that the *n*-propoxide and *iso*-propoxide of sodium prepared are free of alcohol and moisture. The purity of these alkoxides is confirmed by elemental analysis and powder XRD technique. The results obtained from CHNS analyser and AES methods are reported elsewhere [17]. The present work reports the IR spectra and XRD patterns of these compounds for the first time.

Fig. 2(a) and (b) shows the typical data obtained from TGA-MS system for the decomposition of sodium *n*-propoxide and sodium *iso*-propoxide performed at a linear heating rate of 5 K min^{-1} under argon atmosphere. The figures show the change in sample weight (TG trace) and intensity of gaseous products formed (MS measurement) during the decomposition as a function of specimen temperature. The decomposition patterns obtained under other heating rates of 3 and 10 K min^{-1} are also similar except for the usual increase in the observed decomposition temperatures with increase in heating rate.

The initial weight gain as seen in Fig. 2(a) and (b) of TG trace is due to the absorption of atmospheric moisture by the sample while loading. The first weight loss observed around 366 and 350 K are due to the evaporation of *n*-propanol and *iso*-propanol, respectively, which are formed by the reaction of respective sodium alkoxides with moisture picked up by the sample during loading into the TGA-MS system. This is confirmed by heating fresh compound of sodium *n*-propoxide and sodium *iso*-propoxide separately up to 450 K and subjecting the residue to XRD

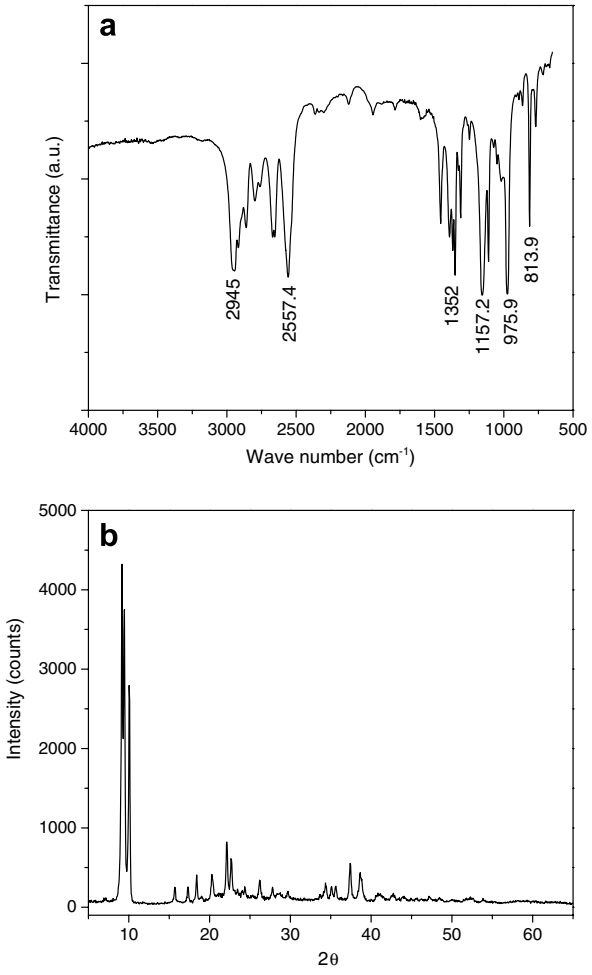

Fig. 1. (a) IR spectrum and (b) XRD pattern of sodium *iso*-propoxide.

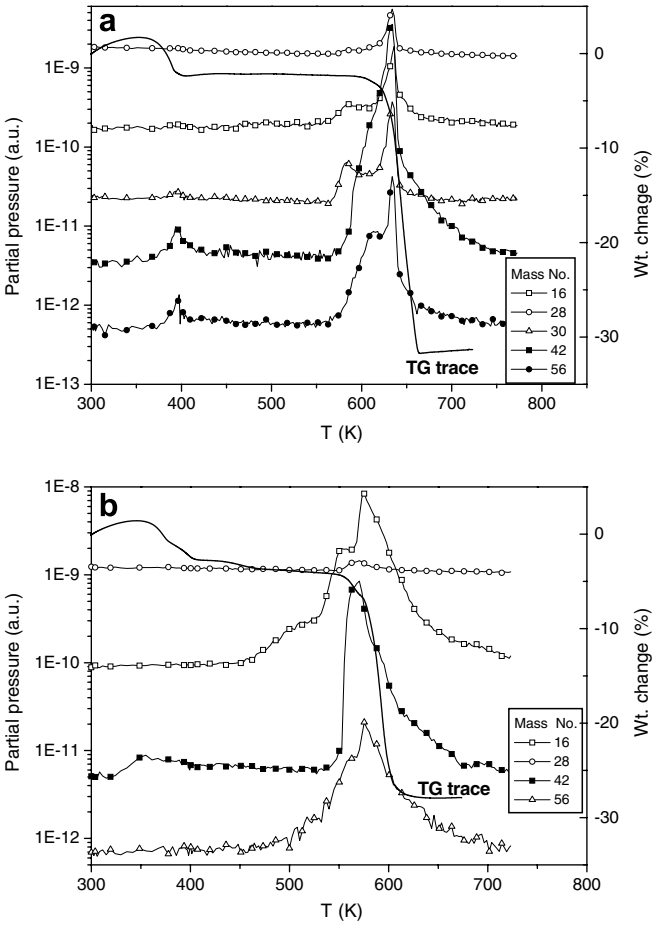

Fig. 2. Typical TGA-MS curve for decomposition of (a) sodium *n*-propoxide and (b) sodium *iso*-propoxide at a heating rate of 5 K min^{-1}.

and IR analysis. The XRD pattern and IR spectra obtained for the residue matched exactly with that of the pure compound.

The decomposition of sodium *n*-propoxide starts above 590 K (Fig. 2(a)). The rate of the decomposition up to 625 K is slow in the beginning and becomes faster beyond 625 K, which is reflected in the slope as shown in Fig. 6(a). The gaseous products formed on decomposition are mainly propylene (mass: 42), and butylene (mass: 56) with minor quantities of methane (mass: 16), ethane (mass: 30) and very small quantity of ethylene (mass: 28). Even though quantitative estimation of the gaseous products formed was not possible with the present set-up, qualitatively it can be seen from the mass spectrum recorded simultaneously for the evolved gases as shown in Fig. 2(a). The lines corresponding to propylene and butylene show that their quantities increased by 3 and 2 orders, respectively. The solid residue was found to be a mixture of sodium carbonate, sodium hydroxide and amorphous carbon.

The decomposition of sodium *iso*-propoxide is observed to start above 550 K (Fig. 2(b)). In this case too the decomposition is slower in the beginning and there after decomposed at a faster rate as shown in Fig. 7(a). The gaseous products formed on decomposition are mainly methane (mass: 16), propylene (mass: 42) and butylene (mass: 56) with minor quantity of ethylene (mass: 28). Formation of methane is high when compared to that of propylene and butylene. In this case also the solid residue was found to be a mixture of sodium carbonate, sodium hydroxide and amorphous carbon.

The formation of higher amounts of propylene in the case of sodium *n*-propoxide decomposition and higher amounts of methane in the case of *iso*-propoxide decomposition can be ascribed to the normal and branched chain of the alkyl group. Decomposition of sodium *iso*-propoxide follows the pattern similar to that of sodium ethoxide, where methane was found to be in major quantity [18]. The weight loss observed for *n*-propoxide and *iso*-propoxide were 29 and 24 wt%, respectively. The high weight loss in the case of *n*-propoxide decomposition could be due to straight chain and the lower weight loss in the case of *iso*-propoxide resulted in higher insoluble content as free carbon.

Being of same molecular weight, the unequivocal determination of formation of carbon monoxide and ethylene, either individually or combined, during the decomposition of these alkoxides is beyond the capability of the present MS system. However, this isobaric interference is generally overcome by using their respective finger print mass spectra and also by IR analysis of the gases. Thus it was confirmed that the mass 28 observed in the present case corresponds only to ethylene and not to carbon monoxide.

Sodium *n*-propoxide and sodium *iso*-propoxide on decomposition, produce saturated and unsaturated gaseous hydrocarbons with black dry powdery residue. Various techniques such as XRD, IR and volumetric analysis are used to characterize the residue.

Powder XRD patterns of the decomposition residues of these sodium alkoxides are shown in Fig. 3(a) and (b). All the peaks are identified and found to match well with those of sodium carbonate and sodium hydroxide pattern reported in the literature [19,20]. The XRD pattern of the water and HCl insoluble black particles exhibited only background spectra except a broad hump at 20°. This indicates that the insoluble residue is amorphous carbon.

IR spectra of the decomposition residues of sodium *n*-propoxide, sodium *iso*-propoxide and commercially available sodium carbonate are shown in Fig. 4(a) and (b) along with the IR spectrum of a commercial sodium carbonate sample in Fig 4(c), for comparison. The spectral features around 1450 and 870 cm^{-1} obtained for the residues match exactly with that of sodium carbonate recorded in the present work and also with that reported in the literature [21]. This confirms that the residues contain sodium carbonate. The IR spectra of insoluble black particles did not show any spectral feature of C–C or C–H bonding. It is clear that the black particles are free of hydrocarbon.

Addition of dilute hydrochloric acid to the decomposition residues produced brisk effervescence and the subsequent standard lime water test confirmed the presence of carbonate in the decomposition residues of sodium *n*-propoxide and sodium *iso*-propoxide.

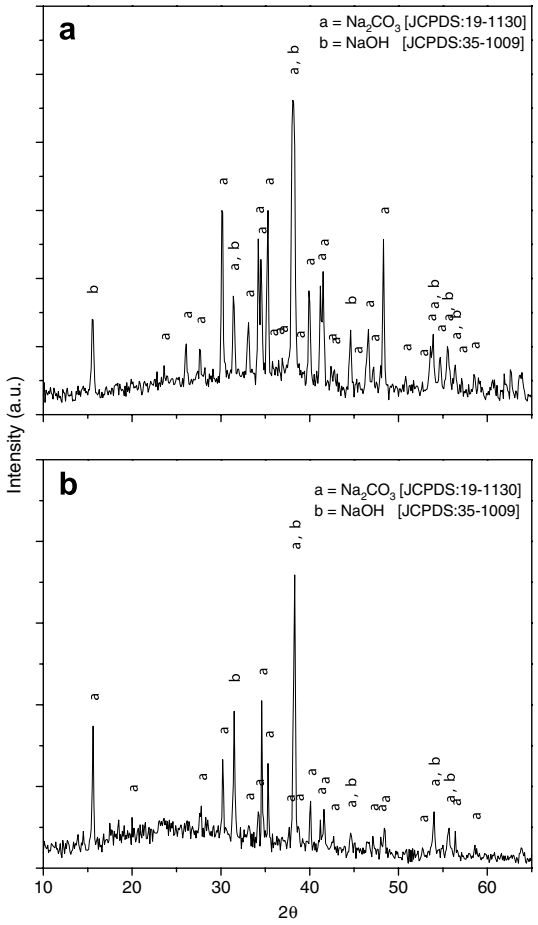

Fig. 3. XRD pattern for decomposition residues of (a) sodium *n*-propoxide and (b) sodium *iso*-propoxide.

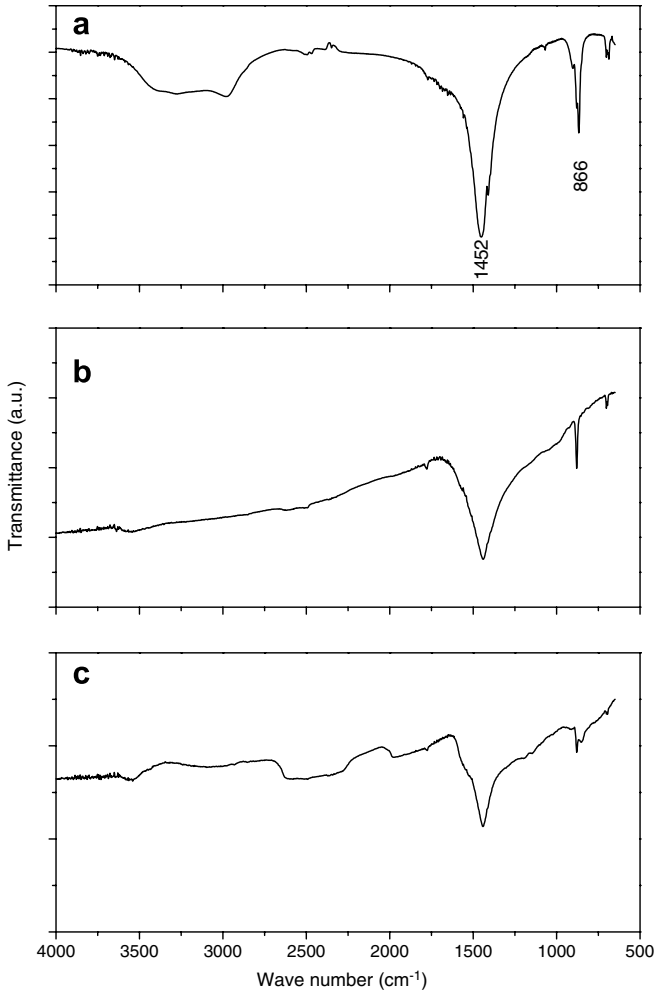

Fig. 4. IR spectra of (a) sodium carbonate, (b) decomposition residue of sodium *n*-propoxide and (c) decomposition residue of sodium *iso*-propoxide.

The quantities of sodium carbonate and sodium hydroxide in the residue were estimated by volumetric titration and the results obtained are given in Table 1. The results indicated that the decomposition residues contained sodium carbonate and sodium hydroxide in the mole ratio of 1:2. The total sodium content contributed by sodium carbonate and sodium hydroxide are given in Table 1 which is in good agreement with the percentage of weight loss obtained by TGA data.

The weight percent of soluble and insoluble portions of the decomposition residues of sodium *n*-propoxide and sodium *iso*-propoxide in distilled water and in hydrochloric acid were same and are given in Table 1. It is clear that the weight percent of soluble portions of the solid residue are due to the sodium carbonate and sodium hydroxide. The measured weight percent of free carbon and carbon contributed by sodium carbonate are in close agreement with those estimated by CHNS analyzer.

From all these observations, the possible decomposition reaction for the sodium alkoxide can be written as follows:

$$\mathrm{RONa} \rightarrow m\mathrm{Na_2CO_3} + x\mathrm{C} + 2m\mathrm{NaOH} + yC_nH_{2n+2} + zC_nH_{2n} \quad (3)$$

where m, x, y, and z are constants and n the number of carbon atoms present in the hydrocarbon. $x = 4$ in the case of *n*-propoxide and 5 for *iso*-propoxide decomposition; R denotes normal and *iso*-propyl group of the two alkoxides.

4. Kinetic analyses

Kinetic analysis of the TGA and MS data of the decomposition of sodium alkoxides was done to arrive at the possible mechanism of dissociation and association processes and to deduce the kinetic parameters. In the present study, the kinetic parameters were evaluated by employing the model dependent method.

Since the reaction rate (r) is proportional to the amount of reactant at any time, t, it can be expressed by the following relation [22]:

$$r = \frac{\mathrm{d}\alpha}{\mathrm{d}t} = f(\alpha)k(T), \quad (4)$$

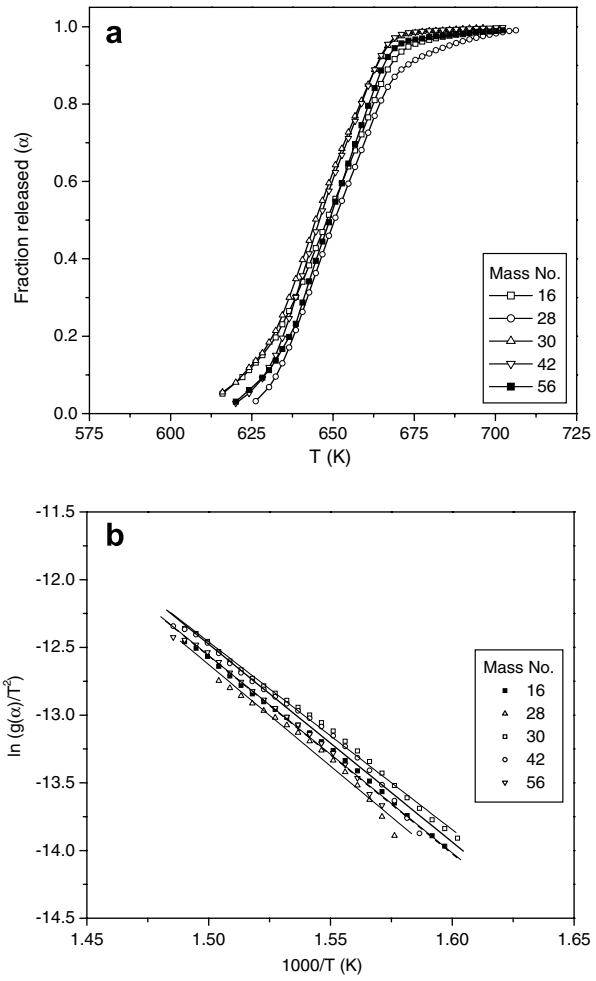

Fig. 5. (a) Plot of fraction formed against temperature deduced from MS data and (b) plot of $\ln(g(\alpha)/T^2)$ versus $1/T$ for sodium *n*-propoxide.

where α represents the extent of conversion of the reactant at time t, $f(\alpha)$ the conversion function which generally represents the mechanism of the reaction and $k(T)$ the rate constant as a function of temperature. The temperature dependence of the rate constant k, is generally expressed in Arrhenious form as

$$k(T) = A\exp(-E_a/RT), \tag{5}$$

where A is the pre-exponential factor, E_a the activation energy, R the universal gas constant and T the absolute temperature.

The non-isothermal rate equation can be represented as

$$\frac{d\alpha}{dT} = \frac{k(T)}{\beta} f(\alpha), \tag{6}$$

where $\beta(=dT/dt)$ is the linear heating rate, and $d\alpha/dT$ is the temperature derivative of the extent of non-isothermal conversion. Eq. (6) can be represented by its integral form as follows:

$$g(\alpha) = \int_0^{\alpha} \frac{d\alpha}{f(\alpha)} = \frac{A}{\beta}\int_0^{T} \exp(-E_a/RT)dT, \tag{7}$$

where $g(\alpha)$ denotes the integral form of rate expressions. The model $g(\alpha)$ functions corresponding to different reaction mechanisms can be found elsewhere [23]. These expressions are applied for the kinetic analysis of solid state reactions and encompass most common mechanisms. The plot of $\ln(g(\alpha)/T^2)$ versus $1/T$ yields a straight line for the appropriate $g(\alpha)$ function. Activation energy, E_a, and pre-exponential factor, A, are calculated from the slope and intercept, respectively.

4.1. Non-isothermal runs

4.1.1. Mass spectrometric data

In mass spectrometer applications, the α is generally defined as

Table 2
Calculated activation energy (E_a) and pre-exponential factor (A) under non-isothermal conditions from MS data

Compound	Product	Heating rate (K min^{-1})	Activation energy E_a (kJ mol^{-1})	Pre-exponential factor A (min^{-1})	Correlation coefficient	Standard deviation
Sodium *n*-propoxide	Methane	0[a]	**154.05 ± 1.36**	**6.42×10^{6}**		
		3	135.59 ± 0.91	1.52×10^{5}	0.9995	0.009
		5	121.15 ± 1.6	1.09×10^{4}	0.9979	0.036
		10	90.12 ± 1.91	2.15×10^{1}	0.9968	0.038
	Ethylene	0[a]	**153.49 ± 2.12**	**6.35×10^{6}**		
		3	134.46 ± 6.07	1.50×10^{5}	0.987	0.040
		5	124.58 ± 5.06	1.89×10^{4}	0.9886	0.054
		10	92.74 ± 2.28	3.61×10^{1}	0.9955	0.050
	Ethane	0[a]	**148.99 ± 6.69**	**4.62×10^{6}**		
		3	134.09 ± 2.59	2.26×10^{5}	0.9959	0.042
		5	115.29 ± 1.53	4.20×10^{3}	0.9981	0.030
		10	90.83 ± 2.66	2.99×10^{1}	0.9932	0.062
	Propylene	0[a]	**143.92 ± 1.86**	**1.72×10^{6}**		
		3	129.00 ± 2.45	8.08×10^{4}	0.9955	0.051
		5	121.52 ± 3.21	1.27×10^{4}	0.9931	0.055
		10	96.54 ± 2.52	7.68×10^{1}	0.9956	0.046
	Butylene	0[a]	**146.42 ± 0.04**	**1.45×10^{6}**		
		3	131.44 ± 3.26	7.19×10^{4}	0.9954	0.02
		5	121.51 ± 2.43	1.16×10^{4}	0.9966	0.033
		10	93.00 ± 2.52	7.68×10^{1}	0.9956	0.046
Sodium *iso*-propoxide	Methane	0[a]	**128.99 ± 0.62**	**7.74×10^{5}**		
		3	119.56 ± 5.27	1.14×10^{5}	0.9858	0.032
		5	114.10 ± 4.43	5.75×10^{4}	0.9940	0.075
		10	98.36 ± 4.45	2.44×10^{3}	0.9939	0.052
	Ethylene	0[a]	**133.62 ± 0.45**	**3.72×10^{6}**		
		3	125.40 ± 8.94	4.84×10^{5}	0.985	0.036
		5	120.51 ± 9.98	2.79×10^{5}	0.977	0.079
		10	106.78 ± 5.96	8.96×10^{3}	0.998	0.021
	Propylene	0[a]	**130.14 ± 0.13**	**1.01×10^{6}**		
		3	123.33 ± 4.09	5.78×10^{5}	0.9941	0.034
		5	118.96 ± 6.86	1.07×10^{5}	0.9886	0.049
		10	107.61 ± 3.30	4.5×10^{4}	0.9985	0.049
	Butylene	0[a]	**130.38 ± 1.44**	**5.37×10^{5}**		
		3	114.47 ± 4.40	2.37×10^{4}	0.9856	0.046
		5	101.96 ± 4.96	4.30×10^{3}	0.9953	0.019
		10	75.53 ± 5.61	2.33×10^{1}	0.9731	0.110

[a] Values extrapolated to zero heating rate.

$$\alpha_{(T)} = \frac{Q_{(T)}}{Q_{(Total)}}, \tag{8}$$

$$= \frac{A_{(T)}}{A_{(Total)}}, \tag{9}$$

where $Q_{(T)}$ and $Q_{(Total)}$ pertain to instantaneous and total quantities of gas released which correspond to area under the release curves $A_{(T)}$ and $A_{(Total)}$, respectively. Detailed measurement of experimental $\alpha_{(T)}$ is described elsewhere [24].

Fig. 5(a) shows the typical plot of fraction formed (α) versus temperature for various gaseous products of decomposition of sodium *n*-propoxide at a linear heating rate of 5 K min^{-1}. Similar plots were also made for other heating rates of sodium *n*-propoxide and sodium *iso*-propoxide. Plots of $\ln(g(\alpha)/T^2)$ against $1/T$ are shown in Fig. 5(b) for the decomposition of sodium *n*-propoxide. The best fit, with high correlation coefficient and less standard deviation, for various $g(\alpha)$ values is selected to represent the possible controlling mechanism. In the present case it was found to match with A2 Avrami–Erofe'ev nucleation and growth model [23]. The physical significance of this model is described elsewhere [18]. From the slope and intercept values, the activation energies and pre-exponential factors are calculated for different heating rates and are given in Table 2.

4.1.2. Thermogravimetric data

In thermogravimetric applications the α is generally defined as

$$\alpha = \frac{(W_t - W_i)}{(W_f - W_i)}, \tag{10}$$

where W is the weight of the sample and the subscripts i, t and f refer to the values at the beginning, at time t and at the end of the reaction, respectively.

Figs. 6(a) and 7(a) show the plots of fraction decomposed, α, versus temperature deduced from the TGA data obtained by non-isothermal runs at different heating rates of sodium *n*-propoxide and sodium *iso*-propoxide, respectively. The plot of $\ln(g(\alpha)/T^2)$ versus $1/T$ gives a straight line when the correct $g(\alpha)$ function is used in Eq. (7). Plots of $\ln(g(\alpha)/T^2)$ versus $1/T$ derived from TGA data are shown in Figs. 6(b) and 7(b). As in the case of MS data, the $g(\alpha)$ function that provides best fit with high correlation coefficient and low standard deviation is selected to

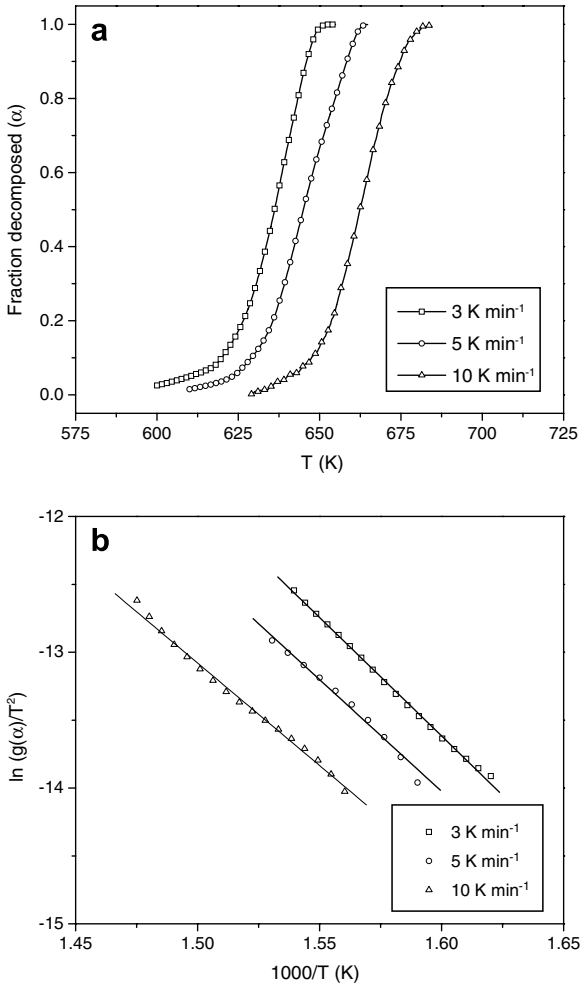

Fig. 6. (a) Plot of fraction decomposed against temperature deduced from TGA trace and (b) plot of $\ln(g(\alpha)/T^2)$ versus $1/T$ for sodium *n*-propoxide.

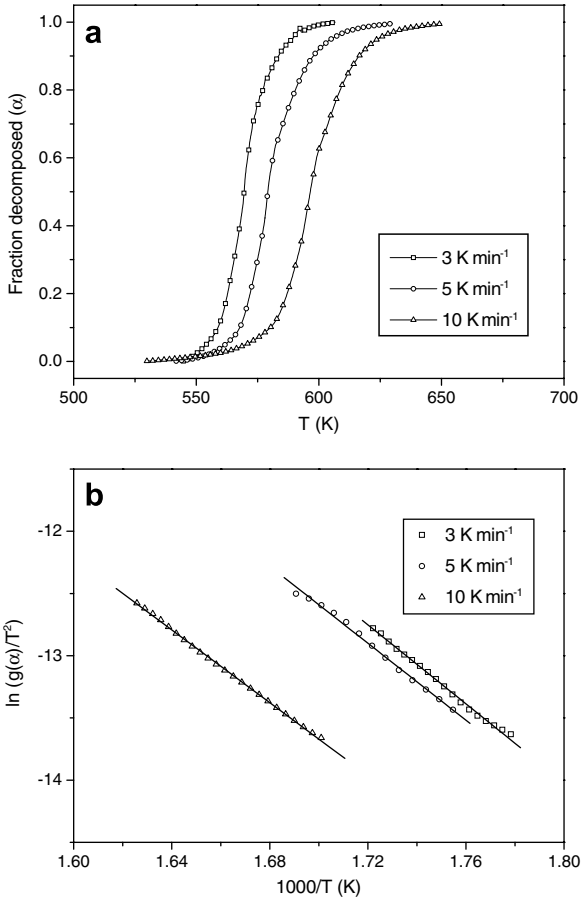

Fig. 7. (a) Plot of fraction decomposed against temperature deduced from TGA trace and (b) plot of $\ln(g(\alpha)/T^2)$ versus $1/T$ for sodium *iso*-propoxide.

Table 3
Calculated activation energy (E_a) and pre-exponential factor (A) under non-isothermal conditions from TGA data

Compound	Mechanism[b]	Heating rate (K min^{-1})	Activation energy E_a (kJ mol^{-1})	Pre-exponential factor A (min^{-1})	Correlation coefficient	Standard deviation
Sodium *n*-propoxide	A2	0[a]	151.94 ± 2.68	**8.58×10^6**		
		3	145.04 ± 0.29	1.61×10^6	0.9993	0.015
		5	136.89 ± 0.97	2.24×10^5	0.9953	0.029
		10	125.54 ± 0.53	1.43×10^4	0.9971	0.029
Sodium *iso*-propoxide	A2	0[a]	**136.14 ± 0.34**	**9.26×10^6**		
		3	131.92 ± 0.57	2.06×10^6	0.9984	0.015
		5	128.66 ± 0.61	9.07×10^5	0.9973	0.022
		10	121.64 ± 0.22	7.33×10^4	0.9996	0.009

[a] Values extrapolated to zero heating rate.
[b] A2 refers to Avrami–Erofe'ev nucleation and two dimensional growth model.

represent the possible rate controlling mechanism. The best fit for the decomposition of all the sodium alkoxides is obtained from A2 Avrami–Erofe'ev nucleation and growth model. The corresponding activation energies and pre-exponential factors are then calculated from the slope and intercept of the above plots and are given in Table 3.

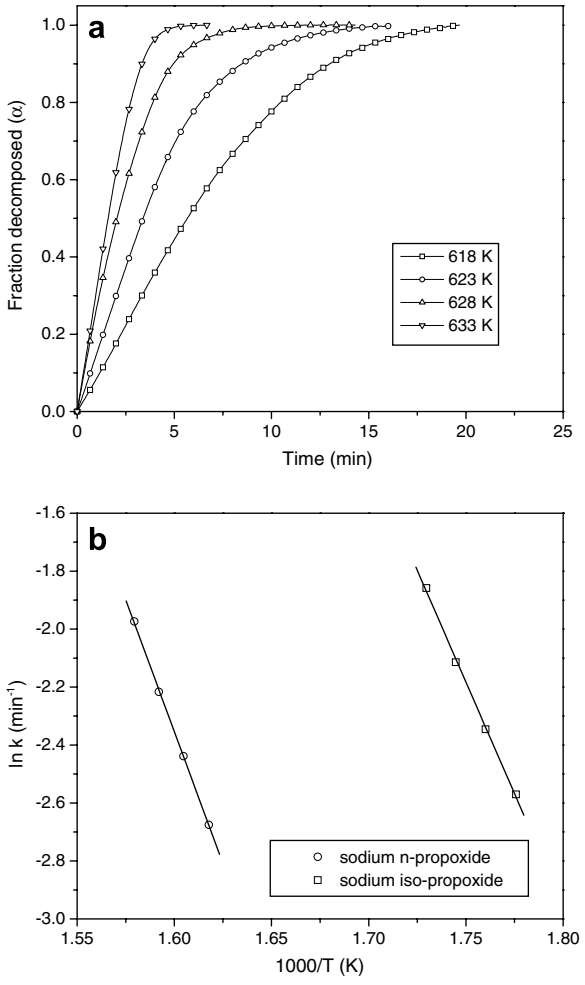

Fig. 8. (a) Plot of fraction decomposed against temperature deduced from TGA trace (isothermal run) for the decomposition of sodium *n*-propoxide and (b) plot of $\ln k$ versus $1/T$.

These values are in good agreement with the values obtained from MS data.

Theoretically, the activation energy of a process is expected not to change with change in heating rate. However, as it had been found and reported earlier [25–28] we have also observed a decrease in activation energy with increase in heating rate. The activation energy values obtained from TG and MS data at different heating rates were plotted as a function of heating rate. A linear fit of this data is extrapolated to zero heating rate and from its intercept the activation energy, which is equivalent to the activation energy arrived by isothermal experiments was calculated and shown in Tables 2 and 3. The similar magnitude in the extrapolated activation energy values obtained for different product gases highlight that they are formed simultaneously and from the same decomposition reaction, which is also seen from TGA-MS spectra (Fig. 2(a) and (b)).

4.2. Isothermal experiments

4.2.1. TG studies

Isothermal experiments were carried out to validate the reaction mechanisms and kinetic parameters deduced from non-isothermal experiments. The fraction formed, α, derived from the isothermal decomposition runs of sodium *n*-propoxide at different temperatures are shown in

Table 4
Values of the rate constants at different temperatures for the decomposition of sodium alkoxides

Compound	Mechanism[a]	Temperature (K)	Rate constant (K min^{-1})
Sodium *n*-propoxide	A2	618.15	6.89×10^{-2}
		623.15	8.73×10^{-2}
		628.15	1.09×10^{-1}
		633.15	1.39×10^{-1}
Sodium *iso*-propoxide	A2	563.15	7.65×10^{-2}
		568.15	9.58×10^{-2}
		573.15	1.21×10^{-1}
		578.15	1.56×10^{-1}

[a] A2 refers to Avrami–Erofe'ev nucleation and two dimensional growth model.

Table 5
Calculated activation energy (E_a) and pre-exponential factor (A) under isothermal conditions from TGA data

Compound	Mechanism[a]	Activation energy E_a (kJ mol^{-1})	Pre-exponential factor A (min^{-1})	Correlation coefficient	Standard deviation
Sodium *n*-propoxide	A2	151.45 ± 2.16	4.32×10^{11}	0.9998	0.007
Sodium *iso*-propoxide	A2	128.07 ± 3.44	5.75×10^{10}	0.9993	0.014

[a] A2 refers to Avrami–Erofe'ev nucleation and two dimensional growth model.

Fig. 8(a). Similar plots were also made for sodium *iso*-propoxide decomposition. The integral form of the isothermal kinetic equation is represented as

$$g(\alpha) = kt, \tag{11}$$

where k is the rate constant at a particular temperature and t the time. Various $g(\alpha)$ functions are plotted against time and the best fit with high correlation coefficient and less standard deviation is taken as the most appropriate mechanism of decomposition. As in non-isothermal experiments, Avrami–Erofe'ev A2 nucleation and growth model gives the best fit. The slope of the curve gives the rate constant, k, of decomposition reaction at a particular temperature. The rate constants obtained at different temperatures are given in Table 4. The natural logarithm of rate constants is plotted against $1/T$ and is shown in Fig. 8(b). The activation energies for the decomposition of sodium *n*-propoxide and *iso*-propoxide are calculated from the slope of these plots using the Arrhenius equation and are given in Table 5.

The activation energies derived from non-isothermal experiments by both TGA and MS techniques are in good agreement with those calculated from isothermal runs. This confirms the validity of the reaction mechanism deduced for the decomposition of sodium *n*-propoxide and sodium *iso*-propoxide.

5. Conclusions

Sodium *n*-propoxide and sodium *iso*-propoxide were prepared and their decomposition is investigated. Thermal decomposition of sodium *n*-propoxide and *iso*-propoxide starts above 623 and 573 K, respectively.

Solid and gaseous decomposition products of sodium *n*-propoxide and sodium *iso*-propoxide were identified and reported for the first time. Solid residues of both alkoxides contain sodium carbonate, sodium hydroxide and free carbon. The mole ratio of sodium carbonate and sodium hydroxide is 1:2. The gaseous products formed on decomposition of sodium *n*-propoxide are mainly propylene and butylene with minor quantities of methane, ethane and very small quantity of ethylene. However, in the case of sodium *iso*-propoxide decomposition, methane, propylene and butylene were the major constituents with ethylene forming in minor quantity.

The activation energies of the decomposition reactions of sodium *n*-propoxide and sodium *iso*-propoxide are found to be 150 and 130 kJ mol^{-1} respectively and are reported for the first time in this study.

The decomposition temperatures of these alkoxides are well above the boiling point of propanol isomers and melting point of sodium (normally sodium cleaning is carried out below the melting point of sodium). Hence, this study has demonstrated that the lower molecular weight alcohols can safely be used for sodium cleaning purposes. Any unexpected temperature rise up to 550 K during sodium cleaning process, due to the exothermic reaction in an accidental condition, will not lead to thermal decomposition of the alkoxides thus ensuring safety of the cleaning process.

Acknowledgements

The authors are grateful to Dr G. Periaswami, former Head, Materials Chemistry Division, for his constant encouragement throughout the course of the study and useful suggestions during the preparation of this paper. They thank Dr A.K. Tyagi, for extending the experimental (TGA-MS) facility. The authors thank Dr K.S. Viswanathan and Dr K. Sankaran for their help in recording IR spectra. Thanks are due to Dr R. Nithya, for XRD analysis.

References

[1] A.E. Walter, A.B. Reynolds, Fast Breeder Reactors, Pergamon, New York, 1981.
[2] H.U. Borgstedt, C.K. Mathews, Applied Chemistry of the Alkali Metals, Plenum Press, New York and London, 1987.
[3] A. Farmer, J. Inst. Fuel 50 (1977) 23.
[4] J.M. Lutton, R.P. Colburn, F. Welch, Atom. Energy Rev. 18 (4) (1980) 815.
[5] IAEA-Specialists Meeting on Sodium Removal and Decontamination, Washington, February 1978, Report: IWGFR-23, p. 1.
[6] W. Haubold, C.Ch. Smit, K.Ch. Stade, Status of sodium removal and component decontamination technology in the SNR programme, IAEA Specialists Meeting on Sodium Removal and Decontamination, Washington, February 1978, Report: IWGFR-23, p. 1.
[7] W.E. Ruther, C.R.F. Smith, EBR-II experience with sodium cleaning and radioactivity decontamination, IAEA-Specialists Meeting on Sodium Removal and Decontamination, Washington, February 1978, Report: IWGFR-23, p. 182.
[8] D. Jambunathan, M.S. Rao, V.S. Krishnamachari, K.V. Kasiviswanathan, M. Rajan, Experience on Sodium Removal from FBTR Components in its Operating Phase, IAEA/IWGFR-Technical Committee Meeting on Sodium Removal and Disposal from LMFRs in Normal Operation and in the Frame Work of Decommissioning, 3–7 November 1997, France, IWGFR-98.

[9] J.G. Asquith, O.P. Steele, F.H. Welch, Sodium Removal Technology – The alcohol process, Proceeding of International Conference on Liquid Metal Technology in Energy Production, Pennsylvania, May, 1976, p. 548.
[10] K.Ch. Stade, Operating Experience in Cleaning Sodium-Wetted Components at the KNK Nuclear Power Plant, IAEA-Specialists Meeting on Sodium Removal and Decontamination, Washington, February 1978, Report: IWGFR 23, p. 17.
[11] P. Menzenhauer, H.U. Boorgstedt, H.H Stamm, Th. Dippel, S. Kunze, D. Hentschel, Experience with Cleaning of Sodium-Wetted Components and Decontamination at Nuclear Research Centre, Karlsruhe, IAEA-Specialists Meeting on Sodium Removal and Decontamination, Washington, February 1978, Report: IWGFR-23, p. 30.
[12] J.A. Bray, D.M. Donaldson, UK Fast Reactor Components – Sodium Removal Decontamination and Requalification, IAEA-Specialists Meeting on Sodium Removal and Decontamination, Washington, February 1978, Report: IWGFR 23, p. 110.
[13] R. Caponetti, J. Nucl. Technol. 70 (1985) 408.
[14] P. Marmonier, J. Del Negro Cea, Information about the Accident Occurred Near RAPSODIE, IAEA / IWGFR – Technical Committee Meeting on Sodium Removal and Disposal from LMFRs in Normal Operation and in the Frame Work of Decommissioning. 3–7 November 1997, France, IWGFR-98.
[15] J. Minges, W. Cherdron, W. Schutz, Short report of an accident during Sodium Cleanup with Ethyl Carbitol in a Storage Tank of a Research Facility, IAEA/IWGFR – Technical Committee Meeting on Sodium Removal and Disposal from LMFRs in Normal Operation and in the Frame Work of Decommissioning. 3–7 November 1997, France, IWGFR-98.
[16] B.S. Furniss, A.J. Hannaford, V. Rogers, P.W.G. Smith, A.R. Tatchell (Eds.), Vogel's Text Book of Practical Organic Chemistry including Qualitative Organic Analysis, fourth ed., The English Language Book Society and Longman Group, London, 1980, p. 268.
[17] K. Chandran, R. Nithya, K. Sankaran, A. Gopalan, V. Ganesan, Bull. Mater. Sci. 29 (2) (2006) 173.
[18] K. Chandran, M. Kamruddin, P.K. Ajikumar, A. Gopalan, V. Ganesan, J. Nucl. Mater. 358 (2006) 111.
[19] JCPDS – International Centre for Diffraction Data, PDF-2 database 1999, File 19 1130.
[20] JCPDS – International Centre for Diffraction Data, PDF-2 database 1999, File 35 1009.
[21] R.A. Nyquist, R.O. Kagel, Infrared Spectra of Inorganic Compounds, Academic Press, New York, 1971.
[22] C.H. Bamford, C.F.H. Tipper, Comprehensive Chemical Kinetics, vol. 22, Elsevier, Amsterdam, 1980.
[23] M.E. Brown (Ed.), Hand Book of Thermal Analysis and Calorimetry, Vol. 1, Principles and Practice, Elsevier, 1998.
[24] S. Dash, M. Kamruddin, S. Bera, P.K. Ajikumar, A.K. Tyagi, S.V. Narasimhan, Baldev Raj, J. Nucl. Mater. 264 (1999) 271.
[25] E. Urbanvici, E. Segal, Thermochim. Acta 107 (1986) 359.
[26] S.B. Kanungo, S.K. Mishra, Thermochim. Acta 241 (1994) 171.
[27] P.K. Heda, D. Dollimore, K.S. Alexander, D. Chen, E. Law, P. Bicknell, Thermochim. Acta 255 (1995) 255.
[28] Kitheri Joseph, R. Sridharan, T. Gnanasekaran, J. Nucl. Mater. 281 (2000) 129.